

Electronic Supplementary Material (ESI) for Nanoscale.
This journal is © The Royal Society of Chemistry 2024

Electronic Supplementary Information

3D printable liquid metal-based hydrogel for multifunctional epidermal sensor

Jingjiang Wei,^{‡a,f} Hao Chen,^{‡a} Fei Pan,^{‡b} Hongming Zhang,^a Tianyu Yuan,^a Yuanlai Fang,^a Zhongxiang Bai,^a Kun Yang,^a Yidi Li,^c Hang Ping,^{d,f} Yanqing Wang,^{*e} Qingyuan Wang,^{*a} and Zhengyi Fu^{*d,f}

^a Institute for Advanced Study, Chengdu University, Chengdu 610106, P. R. China.

^b Department of Chemistry, University of Basel, Basel 4058, Switzerland.

^c State Key Laboratory of Precision Blasting, Jiangnan University, Wuhan 430100, P. R. China.

^d State Key Laboratory of Advanced Technology for Materials Synthesis and Processing, Wuhan University of Technology, Wuhan 430070, P. R. China.

^e College of Polymer Science and Engineering, Sichuan University, Chengdu 610065, P. R. China.

^f Hubei Longzhong Laboratory, Wuhan University of Technology Xiangyang Demonstration Zone, Xiangyang 441000, P. R. China.

[‡] Those authors contributed equally to this work.

* Email: yanqingwang@scu.edu.cn; wangqy@cdu.edu.cn; zyfu@whut.edu.cn

The Supporting Materials Include:

Experimental section

Figure S1. TEM image of LM nanoparticle coated by PAA.

Figure S2. Ultrasonic dispersion of liquid metal nanoparticles with and without PAA.

Figure S3. The LM@PAA dispersion obtained by ultrasonic and stirring treatment.

Figure S4. SEM image of freeze-dried Ca-PAA-LM hydrogel with EDS mapping of C, O, Ca, Ga and In elements.

Figure S5. Element distribution map of CPL hydrogel.

Figure S6. XRD patterns of Ca-PAA-LM hydrogel, Ca-PAA hydrogel and LM@PAA suspension.

Figure S7. FTIR spectra of Ca-PAA-LM hydrogel, Ca-PAA hydrogel, LM@PAA suspension and PAA solution.

Figure S8. Raman spectra of Ca-PAA-LM hydrogel, Ca-PAA hydrogel and LM@PAA suspension.

Figure S9. XPS surveys of Ca-PAA hydrogel and Ca-PAA-LM hydrogel.

Figure S10. Digital photos of CPL hydrogels with different liquid metal content.

Figure S11. Conductivity of CPL hydrogels with different LM contents.

Figure S12. CPL hydrogels for reusable adhesion to the skin.

Figure S13. Digital photos of epidermal sensor monitoring the limb movement process.

Figure S14. Digital photos of real-time EMG monitoring by LM-based epidermal sensor.

Table S1. Comparison of conductivity of common hydrogels.

References

Movie S1. CPL hydrogel quick self-healing process.

EXPERIMENTAL SECTION

1. Raw materials. Polyacrylic acid (PAA, solution, $M_w = 250000$, 35% in water;) was purchased from Sigma-Aldrich (Shanghai) Trading Co., Ltd. Calcium chloride anhydrous (CaCl_2 , ACS grade, $\geq 96.0\%$) was purchased from Shanghai Titan Scientific Co., Ltd. Eutectic Gallium-Indium alloy (EGaIn, 75% Ga and 25% In by weight) were purchased from Shenyang Jiabei Co., Ltd. Sodium hydroxide (NaOH, AR grade, $\geq 96\%$) was purchased from Shanghai Titan Scientific Co., Ltd. The water purifier prepared the deionized water (DIW) used in all experiments ($18.2 \text{ M}\Omega\cdot\text{cm}$, UPA-L Shanghai Lichen Technology Co., Ltd.).

2. Preparation of Ca-PAA-LM hydrogels. Firstly, adding PAA (1.08 mL) into deionized water (23.92 mL) to prepare PAA solution (0.6 M). Concurrently, a CaCl_2 solution (0.3 M) was prepared by dissolving CaCl_2 powders (0.833 g) in deionized water (25 mL), followed by stirring for 10 min at room temperature. Subsequently, bulk EGaIn (0.375 g) was added to the PAA solution, yielding a 1.5 wt% PAA-LM mixture. This mixture was placed in an ice-water bath, and an ultrasonic probe (10 min, 900 W, 30% amplitude, JY92-II N, Shanghai Li-Chen Technology Co., LTD) was used to obtain uniform LM@PAA suspension. The sonication time was adjusted to control the final droplet size of EGaIn.

For the preparation of the Ca-PAA-LM hydrogel, NaOH solution (50 mL, 0.1 M) was added dropwise to the PAA-EGaIn mixture solution under continuous stirring at 1000 rpm. After the dropwise addition was complete, stirring was continued until a gray-black viscous hydrogel formed and the solution was clarified. The residual solution was discarded, and the final Ca-PAA-LM hydrogel was washed with deionized water.

3. Characterization. The microscopic surface structure of the Ca-PAA-LM hydrogel was observed using scanning electron microscopy (SEM, German ZEISS GeminiSEM 300). For the convenience of observing the surface morphology and porous network structure of the Ca-PAA-LM hydrogel, freeze-drying was performed on all hydrogels using a freeze dryer. The microstructure of hydrogels was studied by transmission electron microscopy (TEM, Thermofisher Talos F200x) with the function of selected area electron diffraction (SAED). Chemical bonds of the hydrogel were studied by X-ray photoelectron spectroscopy (XPS, Thermofisher Nexsa). Phase information and surface chemical states were obtained using an X-ray diffractometer (XRD, Rigaku MiniFlex 600, Japan) at a 5° min^{-1} scanning rate. The hydrogel was analyzed and identified using a Fourier-transform infrared spectrometer (FTIR, Thermo Scientific Nicolet iS20) within the 4000 cm^{-1} to 400 cm^{-1} range. Raman spectroscopy was used to analyze the composition of hydrogels (Renishaw inVia). The rheological properties of all the inks were measured on a rotational and oscillatory rheometer (Thermo HAAKE MARS 40 machine) using a 20 mm parallel plate top geometry with a 1 mm gap at 20°C . The shear-thinning properties of CPL hydrogels were investigated by rotational test at a controlled shear rate, whereas its yield stress was measured by oscillatory test at controlled strain. The following equation is the relationship between viscosity (shear stress) and shear rate:

$$\eta = K\gamma^{n-1} \quad (1)$$

Where η is the viscosity, γ is the shear rate, K is the flow consistency index, and n is the shear-thinning index. Different shear-thinning indices exist for Newtonian and Fey fluids (Shear-thinning fluids). For Newtonian fluids, $n = 1$; $0 < n < 1$ for shear-thinning fluids.

4. Conductivity measurements. The CPL hydrogel was filled into a cylindrical container with a diameter of 1.2 cm and a height of 6.5 cm. The container was sealed at both ends with copper foil and connected to an LCR meter (TH2830) to detect the resistance changes. The resistivity (ρ) was calculated using the following equation:

$$\rho = R_a S / h \quad (2)$$

Where h is the height of the cylindrical container, R_a is the average resistance value detected over multiple measurements, and S is the cross-sectional area. Therefore, the conductivity (σ) followed the formula:

$$\sigma = 1/\rho \quad (3)$$

5. 3D printing of Ca-PAA-LM hydrogels. 3D printing of Ca-PAA-LM hydrogels was performed on an Eazao3D printer (Chengdu Lixiansanwei Technology Co., Ltd). The printed model was prepared in advance using 3D modeling software (Cinema 4D Release 20, Maxon). The software (UltiMaker-Cura-5.3.0) was used for 3D printing slicing. Extrusion pressure during printing was maintained at 0.45 MPa. CPL hydrogel samples containing 1.5 wt% LM were used for 3D printing because the rheology was just enough to self-support after shear thinning.

6. Demonstration of practical applications. This study was conducted with the help of a volunteer who agreed that the data and images could be published. CPL hydrogel-based sensors were attached to the volunteers' fingers, wrists, and knees to monitor their movements in real-time. In addition, CPL hydrogels were used instead of commercial gel electrophysiological electrode patches to collect ECG/EMG signals, which were analyzed by BL-420N Bio-signal Acquisition and Analysis System (Chengdu Taimeng Software Co., LTD).

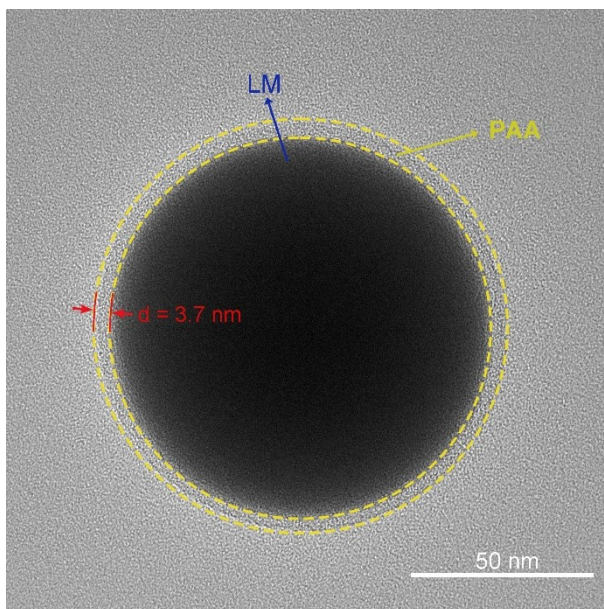


Figure S1. TEM image of LM nanoparticle coated by PAA.

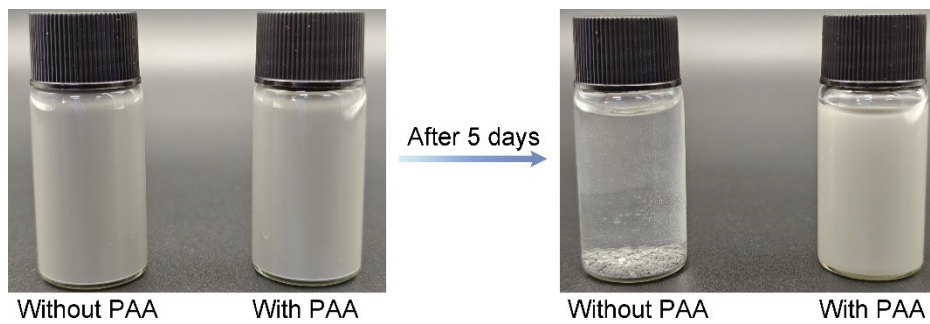


Figure S2. Ultrasonic dispersion of liquid metal nanoparticles with and without PAA.

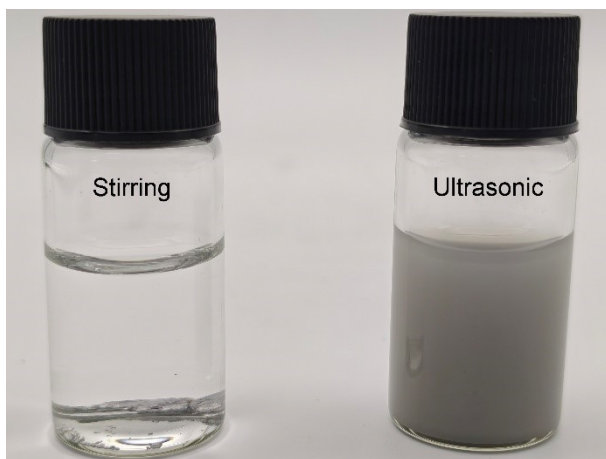


Figure S3. The LM@PAA dispersion obtained by ultrasonic and stirring treatment.

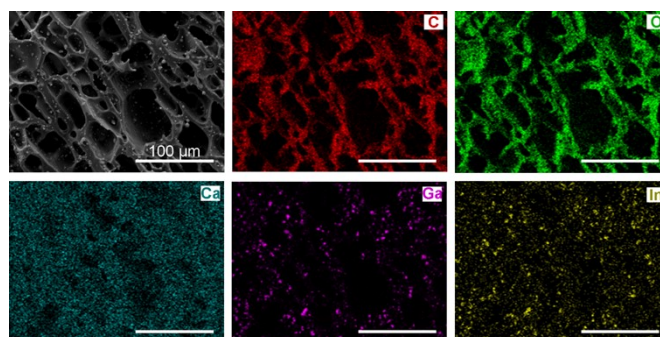


Figure S4. SEM image of freeze-dried Ca-PAA-LM hydrogel with EDS mapping of C, O, Ca, Ga and In elements.

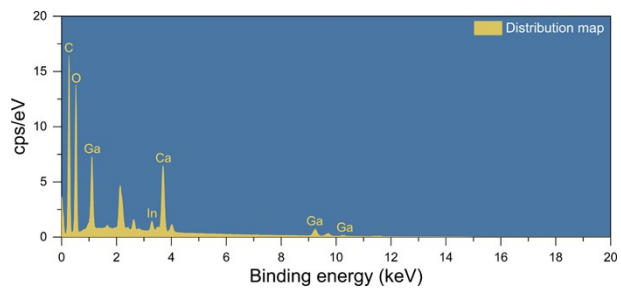


Figure S5. Element distribution map of CPL hydrogel.

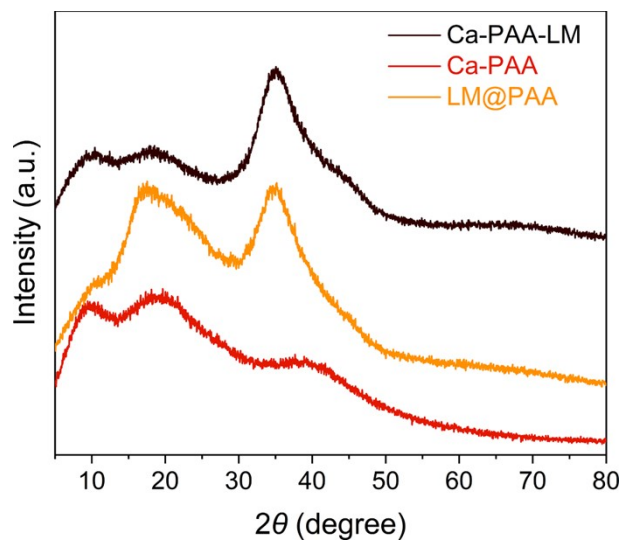


Figure S6. XRD patterns of Ca-PAA-LM hydrogel, Ca-PAA hydrogel and LM@PAA suspension.

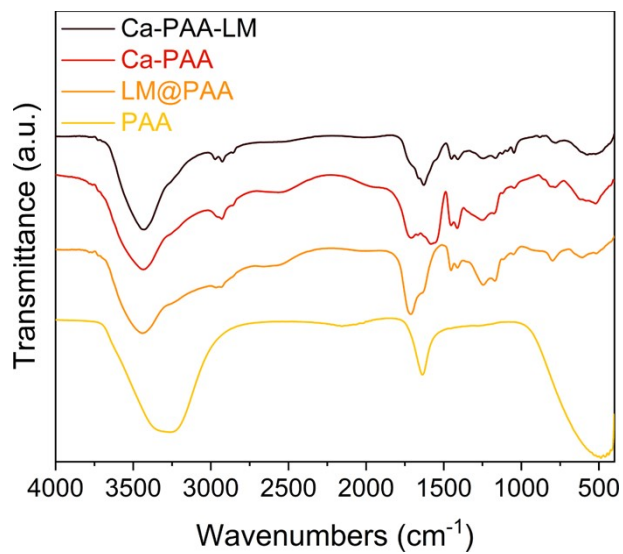


Figure S7. FTIR spectra of Ca-PAA-LM hydrogel, Ca-PAA hydrogel, LM@PAA suspension and PAA solution.

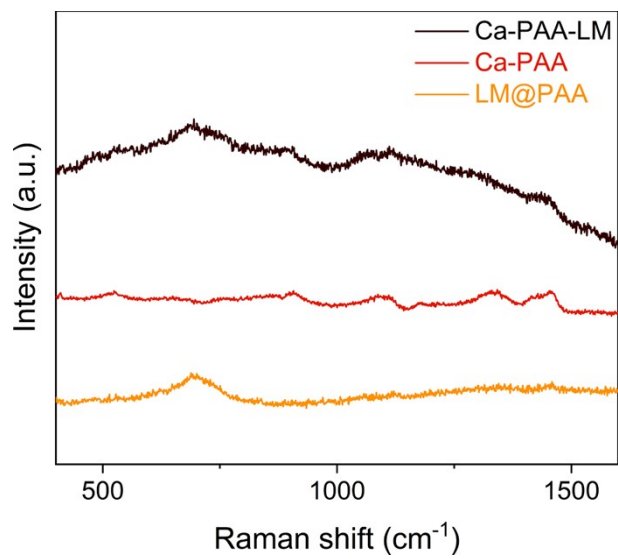


Figure S8. Raman spectra of Ca-PAA-LM hydrogel, Ca-PAA hydrogel and LM@PAA suspension.

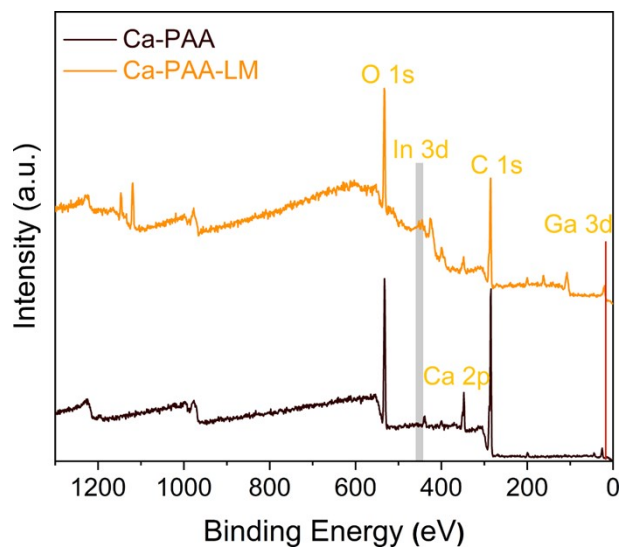


Figure S9. XPS surveys of Ca-PAA hydrogel and Ca-PAA-LM hydrogel.

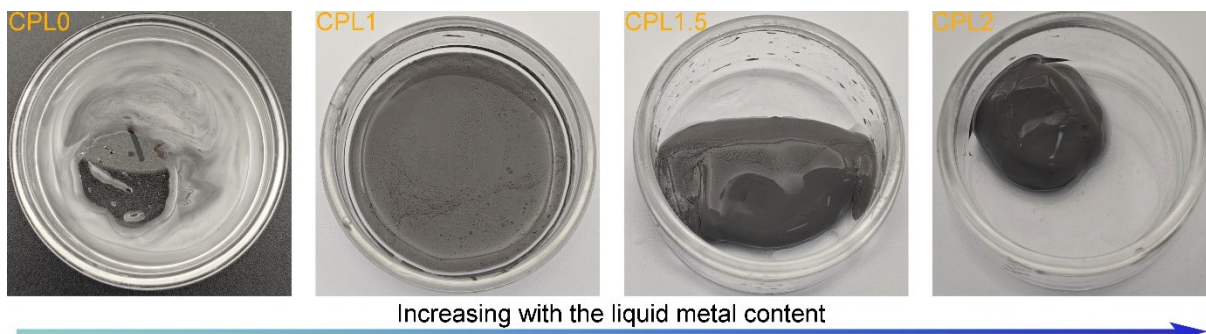


Figure S10. Digital photos of CPL hydrogels with different liquid metal content.

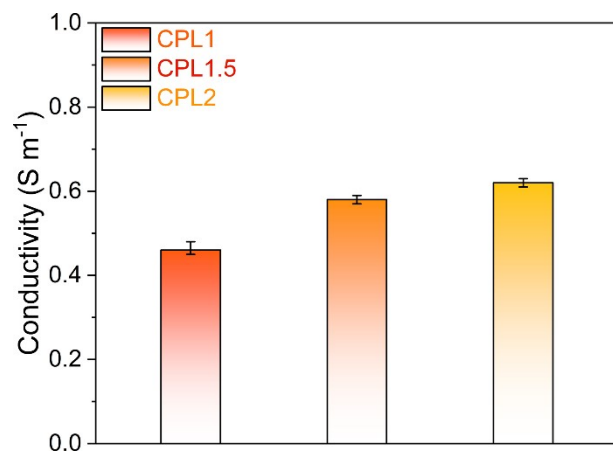


Figure S11. Conductivity of CPL hydrogels with different LM contents.

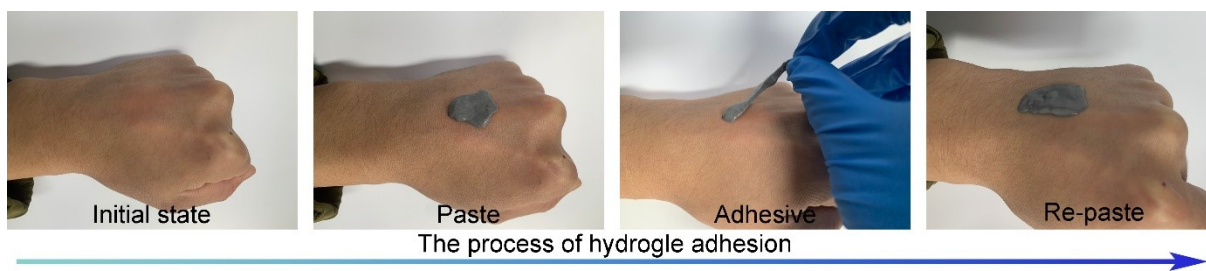


Figure S12. CPL hydrogels for reusable adhesion to the skin.



Figure S13. Digital photos of epidermal sensor monitoring the limb movement process.



Figure S14. Digital photos of real-time EMG monitoring by LM-based epidermal sensor.

Table S1. Comparison of conductivity of common hydrogels.

Materials	Conductivity (S m ⁻¹)	Ref.
PVA/MXene/Py	0.74	1
PAM/lignin-TA/CNC/HPC	0.192	2
CNT/PVA/TA/PAA	0.25	3
CNT/GelMA	0.15	4
GO/PVA	2.15	5
MXene-PAM/Agar	1.02	6
Graphene/PAA/LP/TOCN	~0.56	7
Ca-PAA-EGaIn	~0.62	This work

References

1. Z. Qin, G. Zhao, Y. Zhang, Z. Gu, Y. Tang, J. T. Aladejana, J. Ren, Y. Jiang, Z. Guo, X. Peng, X. Zhang, B. B. Xu and T. Chen, *Small*, 2023, **19**, 2303038.
2. Y. Chen, P. Kuang, Y. Wang, S. Luo, J. Shi, X. Lv, Y. Liu and Q. Fan, *Sci. China Mater.*, 2023, **66**, 4853-4864.
3. K. Park, S. Park, Y. Jo, S. A. Kim, T. Y. Kim, S. Kim and J. Seo, *Ind. Chem. Mater.*, 2024, **2**, 361-377.
4. S. Yao, Y. Yang, C. Li, K. Yang, X. Song, C. Li, Z. Cao, H. Zhao, X. Yu, X. Wang and L.-N. Wang, *Bioacti. Mater.*, 2024, **35**, 534-548.
5. J. Wei, R. Wang, F. Pan and Z. Fu, *Sensors*, 2022, **22**.
6. K. Chen, W. Lai, W. Xiao, L. Li, S. Huang and X. Xiao, *Micromachines*, 2023, **14**.
7. J. Ma, C. Zheng, Y. Lu, Y. Yue, W. Yang, C. Mei, X. Xu, H. Xiao and J. Han, *Compos. Part A Appl. Sci. Manuf.*, 2024, **185**, 108330.